chemosensors

MDPI

Article

Gold Nanoparticles/Carbon Nanotubes and Gold Nanoporous as Novel Electrochemical Platforms for L-Ascorbic Acid Detection: Comparative Performance and Application

Cristina Tortolini [1], Federico Tasca [2], Mary Anna Venneri [1], Cinzia Marchese [1] and Riccarda Antiochia [3,*]

[1] Department of Experimental Medicine, Sapienza University of Rome, Viale Regina Elena 324, 00166 Rome, Italy; cristina.tortolini@gmail.com (C.T.); maryanna.venneri@uniroma1.it (M.A.V.); cinzia.marchese@uniroma1.it (C.M.)
[2] Departamento de Química de los Materiales, Facultad de Química y Biología, Universidad de Santiago de Chile, Casilla 40, Correo 33, Sucursal Matucana, Santiago 9170022, Chile; federico.tasca@usach.cl
[3] Department of Chemistry and Drug Technologies, Sapienza University of Rome, P.le Aldo Moro 5, 00185 Rome, Italy
* Correspondence: riccarda.antiochia@uniroma1.it

Abstract: Herein, the effects of nanostructured modifications of a gold electrode surface in the development of electrochemical sensors for L-ascorbic acid detection have been investigated. In particular, a bare gold electrode has been modified by electrodeposition of gold single-walled carbon nanotubes (Au/SWCNTs) and by the formation of a highly nanoporous gold (h-nPG) film. The procedure has been realized by sweeping the potential between +0.8 V and 0 V vs. Ag/AgCl for 25 scans in a suspension containing 5 mg/mL of SWCNTs in 10 mM $HAuCl_4$ and 2.5 M NH_4Cl solution for Au/SWCNTs modified gold electrode. A similar procedure was applied for a h-nPG electrode in a 10 mM $HAuCl_4$ solution containing 2.5 M NH_4Cl, followed by applying a fixed potential of −4 V vs. Ag/AgCl for 60 s. Cyclic voltammetry and electrochemical impedance spectroscopy were used to characterize the properties of the modified electrodes. The developed sensors showed strong electrocatalytic activity towards ascorbic acid oxidation with enhanced sensitivities of 1.7×10^{-2} μA $\mu M^{-1} cm^{-2}$ and 2.5×10^{-2} μA $\mu M^{-1} cm^{-2}$ for Au/SWCNTs and h-nPG modified electrode, respectively, compared to bare gold electrode (1.0×10^{-2} μA $\mu M^{-1} cm^{-2}$). The detection limits were estimated to be 3.1 and 1.8 μM, respectively. The h-nPG electrode was successfully used to determine ascorbic acid in human urine with no significant interference and with satisfactory recovery levels.

Keywords: L-ascorbic acid; single walled-carbon nanotubes; nanoporous gold; modified electrode; electrochemical characterization; electrochemical sensor

Citation: Tortolini, C.; Tasca, F.; Venneri, M.A.; Marchese, C.; Antiochia, R. Gold Nanoparticles/Carbon Nanotubes and Gold Nanoporous as Novel Electrochemical Platforms for L-Ascorbic Acid Detection: Comparative Performance and Application. *Chemosensors* **2021**, *9*, 229. https://doi.org/10.3390/chemosensors9080229

Academic Editors: Dale A. C. Brownson and Alexey Glushenkov

Received: 26 June 2021
Accepted: 3 August 2021
Published: 16 August 2021

1. Introduction

L-Ascorbic Acid (AA) or vitamin C is a very important compound, that is abundant in many fruits, vegetables and humans [1]. An appropriate amount of this vitamin is especially important for maintaining a healthy immune system. It also plays an important role in wound healing, keeping your bones strong, enhancing brain function and preventing cancer and other diseases, thanks to its antioxidant properties [2–4]. For this reason, the AA content is used as a health indicator [5]. AA cannot be synthetized by the human body, as humans can take AA only from food and integrators. One of the most common reasons people take vitamin C supplements is because, historically, there have been suggestions of the effectiveness of this vitamin to prevent the common cold [6,7]. Moreover, it is known that deficiency of AA can cause scurvy, anemia and premature ageing [8]. European studies have also shown a negative correlation between vitamin C plasma levels and all-cause of cardiovascular mortality [9]. In recent years, emerging literature suggests the role of vitamin C in the treatment of a variety of viral infections [10]. Preliminary

evidence suggests common dietary supplements, such as vitamins C, D and zinc, may help in the fight against COVID-19 [11,12]. Although doctors are using high-dose intravenous (IV) vitamin C, there is no published scientific evidence about the use of IV vitamin C in critically ill COVID-19 patients [13].

Many supplements contain extremely high amounts of this vitamin, which can cause undesirable side effects, such as digestive distress, abdominal cramps, diarrhea and kidney stones [13].

Vitamin C is a water-soluble vitamin, which means it dissolves in water and does not get stored within the body, in contrast to fat-soluble vitamins. Therefore, the vitamin C gets transported to human tissues via body fluids, and any extra gets excreted in urine. However, supplementing with high amounts of vitamin C can lead to adverse effects, because when you overload your body with larger-than-normal doses of vitamin C, it will start to accumulate, potentially leading to overdose symptoms. Normal plasma levels of AA are in the range 4–9 mg/L (25–30 mM). Many diseases are related to changes in its concentration, which should be maintained within this range, avoiding deficiency or excess. The control of vitamin C content in blood or urine is of great importance in clinical diagnostics and, therefore, it is of great interest to develop convenient methods for an accurate detection of AA in biological fluids.

Up to now, several methods have been described for detecting AA including electrophoresis [14,15], spectrophotometry [16,17], chemiluminescence [18–20], oxidation-reduction titration [21,22], HPLC [23–25], fluorescence [26] and electrochemistry [27,28]. Among these methods, electrochemistry is an interesting alternative technique, thanks to its high sensitivity, simplicity, low cost and capability of multiplexing and point-of-care (POC) detection.

The electrochemical detection of AA can be realized with or without incorporation of L-ascorbic acid oxidase enzyme, developing the so-called biosensors or sensors, respectively [29]. Although many examples of enzymatic biosensors are reported in the literature for AA detection, the enzyme-based biosensors are generally affected by enzyme denaturation and/or leaching out from the electrode surface, which can cause short lifetime and instability of the device [30,31]. Moreover, the enzymatic sensors are dependent on oxygen limitations. These drawbacks can be overcome with the development of the enzymeless sensors. The first nonenzymatic sensors were constructed using conventional electrodes, such as glassy carbon (GC), gold (Au) and platinum (Pt). Unfortunately, the electrooxidation of AA at conventional bare electrodes requires a high overpotential (+0.4 V at GC and +0.6 V at both Pt and Au electrodes vs. Ag/AgCl [29]), which causes the adsorption of several organic compounds present in the complex biological samples on the electrode surface, a process called "biofouling", which occurs through the formation of hydrophobic and electrostatic interactions. The biofouling effect can decrease the electron transfer rate and the analytical current signal [32]. A method to overcome this problem is the modification of the electron surface topography by construction of biofouling resistant electrodes with new electrode materials [33,34]. Up to now, thin films [35–39] and nanomaterials [40–44] have been reported for the modification of the electrode surface. In particular, gold-based nanomaterials, such as gold nanoporous, have been successfully investigated for minimizing the electrode biofouling due to protein adsorption [32,45–48] by the size exclusion principle, restricting the transport of large biomolecules within the inner porous surfaces, thus allowing access only to small redox probes.

Highly nanoporous gold (h-nPG), with pore diameter of a few micrometers, drastically increases the electrode surface area and the relative current densities with reduced costs thanks to a lower amount of gold material needed to obtain the same surface area [49,50]. Moreover, the h-nPG film does not require any immobilization procedure on the electrode surface, thus avoiding the drawback of an undesirable loss of material from the surface, as is the case for gold nanoparticles.

Nanoporous gold films are generally fabricated using the following methods: de-alloying, electrochemical deposition and templating [50,51]. The self-templating method is a combined time saving electrochemical-templating method involving two steps: gold electrodeposition and hydrogen bubbling at the electrode, as a self-template, realized by applying a negative potential, usually lower than −3 V vs. SCE [52–55].

In this work, we describe two nano-structured electrochemical sensors for AA detection based on the modification of a bare gold electrode with electrodeposited Au/SWCNTs and self-templating h-nPG, respectively, as represented in Scheme 1. The morphology of the electrodes has been characterized through scanning electron microscopy (SEM), energy dispersive X-ray spectroscopy (EDX), Raman spectroscopy and electrochemical impedance spectroscopy (EIS). The electrochemical characterization of the two sensors has been reported and the analytical performances were compared. Moreover, the potential application of the h-nPG based sensor for testing AA in human urine samples was also investigated.

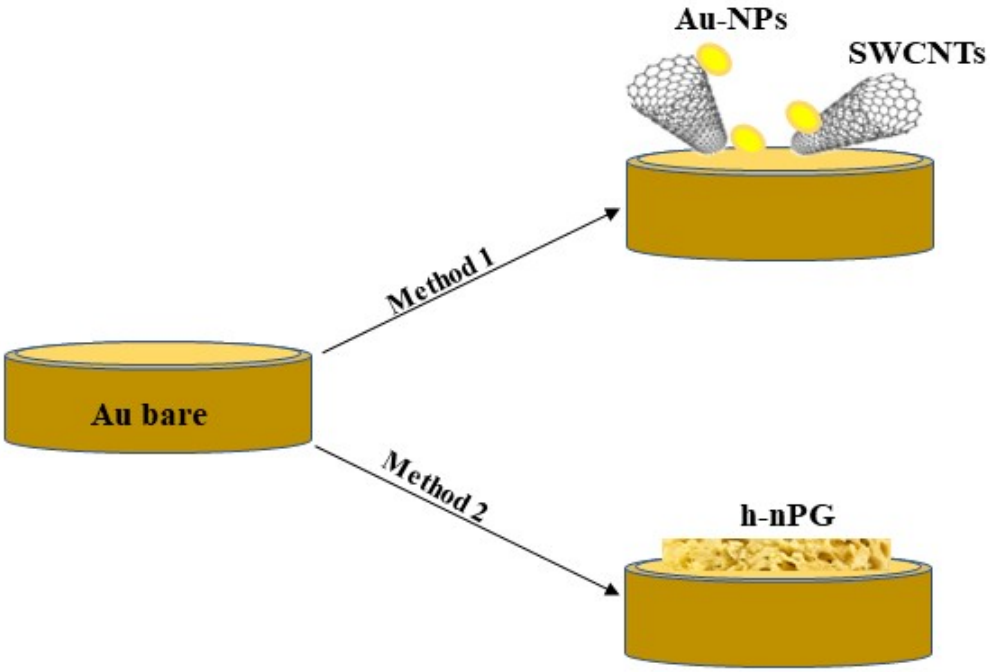

Scheme 1. Schematic representation of the Au/SWCNTs (Method 1) and h-nPG (Method 2). modified gold sensor for ascorbic acid detection.

2. Experimental

2.1. Reagents and Apparatus

L-Ascorbic acid (AA), sodium monobasic phosphate (Na_2HPO_4), sodium dibasic phosphate NaH_2PO_4, potassium chloride (KCl), potassium ferricyanide (III) ($K_3[Fe(CN)_6]$), potassium ferrocyanide (II) ($K_4[Fe(CN)_6]$, gold (III) chloride solution, single-walled carbon nanotubes (SWCNTs, 0.83 nm average diameter) and ammonium chloride (NH_4Cl) were purchased from Sigma-Aldrich (Buchs, Switzerland). All solutions were prepared in a phosphate buffer 0.1 M, KCl 0.1 M, pH 7.4 (PBS buffer). A solution of 1.1 mM $K_3[Fe(CN)_6]$ and 0.1 M KCl in water was used in cyclic voltammetric experiments for determination of electroactive area (A_e) using the Randles-Ševcik equation. High purity deionized water (resistance: 18.2 MΩ cm at 25 °C; TOC < 10 µg L^{-1}) obtained from Millipore (Molsheim, France) has been used throughout experiments.

Electrochemical measurements were performed in a 10 mL thermostated glass cell (model 6.1415.150, Metrohm, Herisau, Switzerland) with a conventional three-electrode configuration with an $Ag/AgCl/KCl_{sat}$ (198 mV vs. NHE) as a reference electrode (catalog number 6.0726.100, Metrohm, Herisau, Switzerland), a glassy carbon rod as counter electrode (cat. 132 6.1248.040, Metrohm, Herisau, Switzerland) and a gold classical electrode (diameter 2 mm) as working electrode (Au, cat. 6.1204.320, Metrohm, Herisau, Switzerland). A gold screen printed electrode, bare and modified (Au-SPE, 220BT Metrohm, (Metrohm Italia, Herisau, Switzerland, Aux: gold; Ref: silver, diameter 4 mm) was also used as working electrode.

Electrochemical impedance (EIS) was utilized to characterize the different modifications of the Au electrode surface. EIS experiments were carried out at equilibrium potential called open circuit potential (OCP) without bias voltage in the frequency range of 0.1–10^3 Hz using an ac signal of 10 mV amplitude at a formal potential of the redox probe (0.22 V vs. Ag/AgCl), using Autolab Potentiostat/Galvanostat (Eco Chemie, Utrecht, The Netherlands). Three-electrode cell configuration with Ag/AgCl as reference electrode and the glassy carbon rod as a counter electrode was used for measures. EIS measurements were carried out using 10 mL of PBS buffer solution containing mixture of 5 mM $Fe(CN)_6^{3-}/Fe(CN)_6^{4-}$, as electrochemical probe.

2.2. Preparation of Gold Modified Electrodes

Au/SWCNTs classical and SPE gold electrodes were modified according to a similar procedure developed in our previous work for MWCNTs, by electrodeposition of Au/SWCNTs sweeping the potential between +0.8 V and 0 V vs SCE for 25 scans at 0.05 Vs^{-1} in a suspension containing 5 mg/mL of SWCNTs in 10 mM $HAuCl_4$ containing 2.5 M NH_4Cl [56,57].

The h-nPG classical and SPE gold electrodes were modified by electrodeposition of h-nPG by initially sweeping the potential for 25 scans between +0.8 V and 0 V vs. Ag/AgCl at 50 mV s^{-1} in a 10 mM $HAuCl_4$ solution containing 2.5 M NH_4Cl. Successively, a fixed potential of −4 V vs. Ag/AgCl was applied to the modified electrode for 60 s in the same solution, in order to allow the formation of pores, due to hydrogen bubbling. Finally, the electrodes were further activated in 0.5 M H_2SO_4, by running CVs between 0 and +1.7 V versus Ag/AgCl at a scan rate of 100 mV s^{-1} for 25 cycles, until a well-defined CV was obtained [58].

2.3. SEM Experiments

A high-resolution field emission scanning electron microscopy (SEM) (HR FESEM, Zeiss Auriga Microscopy, Jena, Germany) was used to investigate the morphology of the modified screen-printed electrodes. All samples were prepared using gold plates (25 Å~25 Å~1 mm, ALS Co. Ltd., Tokyo, Japan) instead of gold electrodes.

In order to evaluate the Au content of the h-nPG modified screen-printed electrode, energy dispersive X-ray spectroscopy (XPS) (Zeiss Auriga Microscopy, Jena, Germany) measurements were performed. The EDX spectrum and data were collected during sample surface scanning by SEM electron probe.

2.4. Raman Spectroscopy

Raman spectra were recorded at room temperature, in back-scattering geometry, with an inVia Renishaw micro-Raman spectrometer (Wotton-under-Edge, Gloucestershire, UK), using the 514.5 nm emission line from an Ar ion laser. The power of the incident beam was about 5 mW. Repeated accumulations (20 scans × 20 s) were acquired on different sample regions using a 50× objective to check sample homogeneity. The spectra were calibrated using the 520.5 cm^{-1} line of a silicon wafer.

3. Results and Discussion

3.1. SEM Characterization

SEM experiments were carried out to investigate the morphology of the Au bare and the Au/SWCNTs and h-nPG modified screen-printed electrodes (Figure 1, panels A–C). In the case of the Au/SWCNTs electrode, it is possible to clearly note the presence of clusters of AuNPs, with a distribution of nanoparticles in the range 50–250 nm diameter, onto the Au electrode surface (Figure 1, panel B). The presence of SWCNTs has been confirmed by Raman spectroscopy (see Section 3.2). The initial reduction of Au^{3+} to Au^{0} with the formation of AuNPs probably facilitated the entrapment of the SWCNTs, allowing a good electrode nanocoating.

As for the h-nPG modified electrode, the honeycomb-like feature with evenly distributed micropores of approximately 10–25 μm in diameter is clearly observed (Figure 1, panel C). The magnified SEM image shows a highly porous branched structure with smaller pores with a diameter of a few hundred nanometers (Figure 1, panel D). The porous structure permeates the gold electrode surface generating the typical sponge-like appearance. It is interesting to note that a negative potential of −4 V vs. Ag/AgCl was necessary for the formation of nucleation centers for the deposition of Au atoms and for the simultaneous evolution of hydrogen bubbling, needed for pore formation. The deposition time of 60 s is quite short compared to a similar method proposed by Kumar et al. [54], where the optimum deposition time was found to be 400 s at the same applied potential, probably thanks to the previous step of potential sweeping, not used in the other work.

In addition, SEM-EDX microanalysis was conducted to support the information obtained with SEM images obtained for the h-nPG film. It shows the presence of only Au element uniformly distributed in the nanoporous structure, indicating the successful formation of the h-nPG film on the surface of the gold electrode (Figure 1, panels D and E).

(**A**)

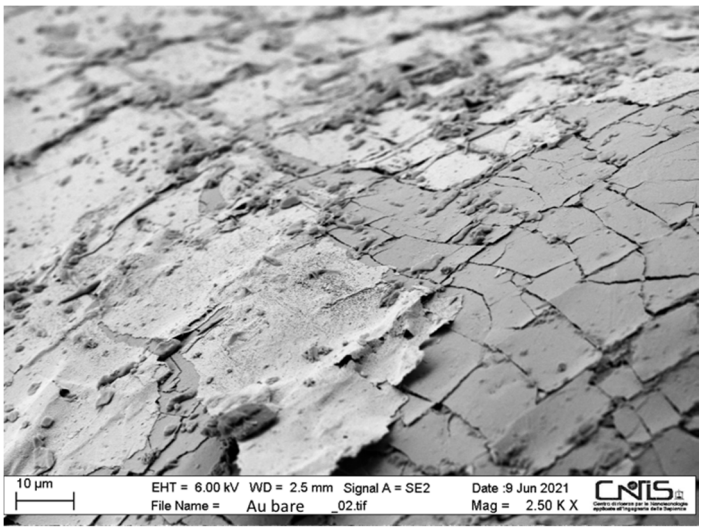

Figure 1. *Cont.*

(**B**)

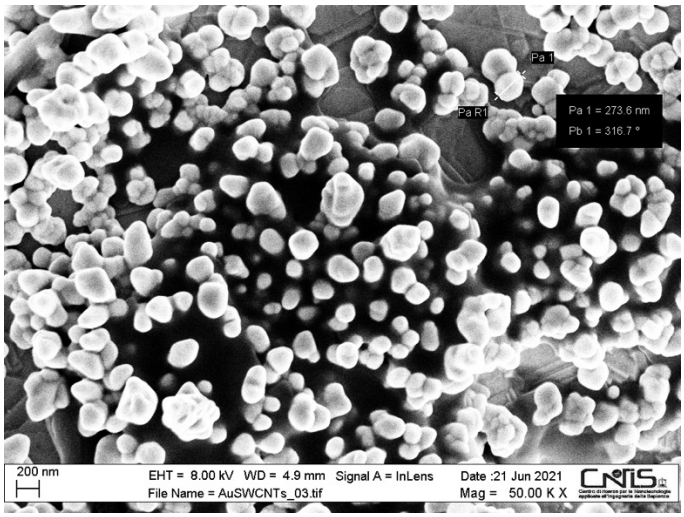

(**C**)

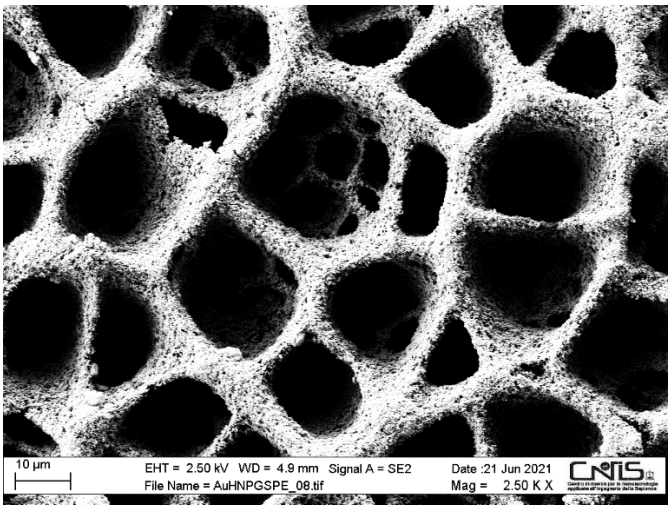

(**D**)

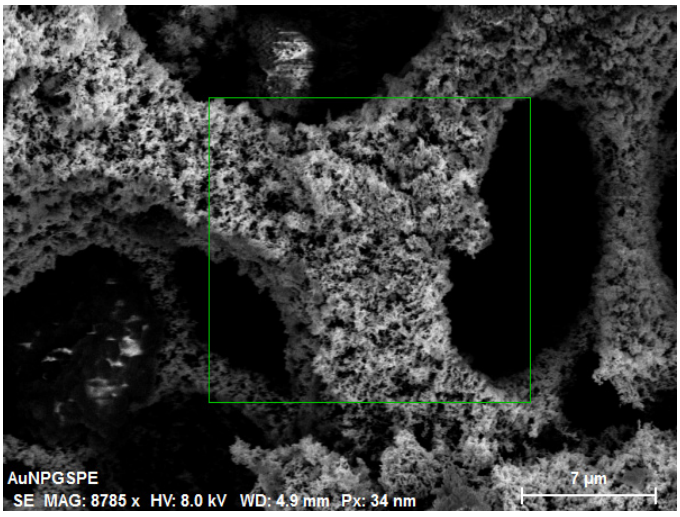

Figure 1. *Cont.*

(**E**)

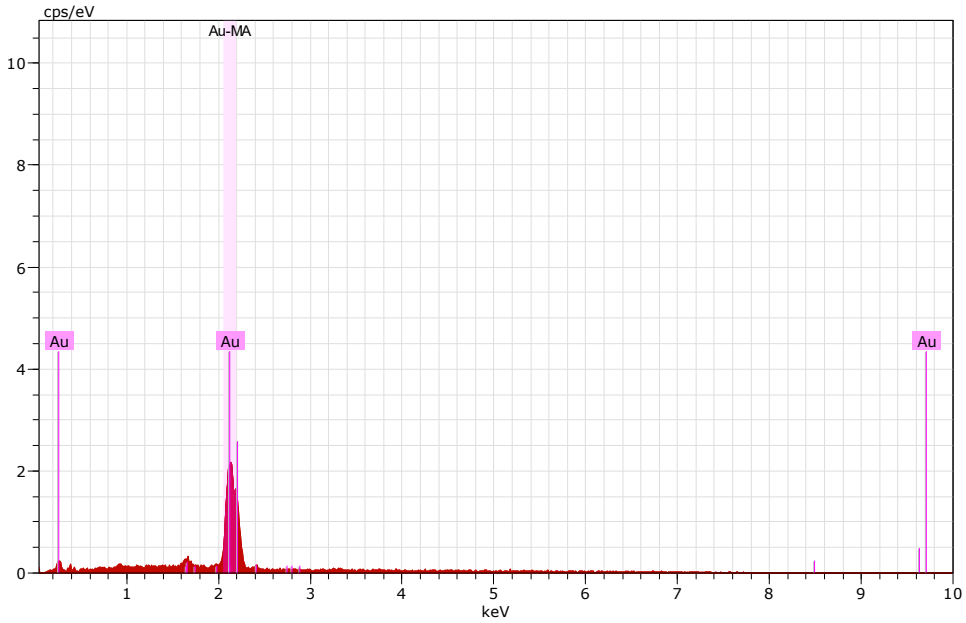

Figure 1. SEM images of bare gold SPE (**A**); Au/SWCNTs gold SPE electrode (**B**) and h-nPG gold SPE electrode (**C**); SEM image of the h-nPG gold SPE electrode with EDX analysis area (**D**); SEM-EDX spectrum of the h-nPG gold SPE electrode (**E**). Magnification: 2500× (**A**), 50,000× (**B**), 2500× (**C**), 8785× (**D**); voltage: 10 kV.

3.2. Raman Characterization

Raman spectroscopy was utilized to demonstrate the presence of SWCNTs onto the Au/SWCNTs modified electrode. The spectra clearly identified the presence of carbon nanotubes (CNTs). Similar spectral profiles were observed in several surface spots, shown in Figure 2. Signals at ~1358, ~1581 and at ~2710 cm^{-1} correspond to the D-(defect, photon-defects interaction), G-(graphite, E_{2g} stretching mode of carbon atoms, and G'-bands (second-order overtone of *D* band), respectively [59]. The absence of radial breathing modes (RBM) in the range 130–400 cm^{-1}, a characteristic of singled-walled carbon nanotubes (SWCTs), could be ascribed to the sharp increase of the background obscuring the low intensity modes. No significant variations of the D-band to the G-band intensity ratios (I_D/I_G, a measure of the structural disorder of the carbon material,) were observed on the spectra of the samples with respect to those of pristine SWCNTs indicating that the dispersion process did not yield an increase of defects.

The sharp bands, marked by a star in Figure 2, at ~450, ~616 and at ~975 cm^{-1} are attributed to sulfate anions adsorbed on surface arising from symmetric bending (v_2), antisymmetric bending (v_4) and symmetric stretching (v_1) modes, respectively [60].

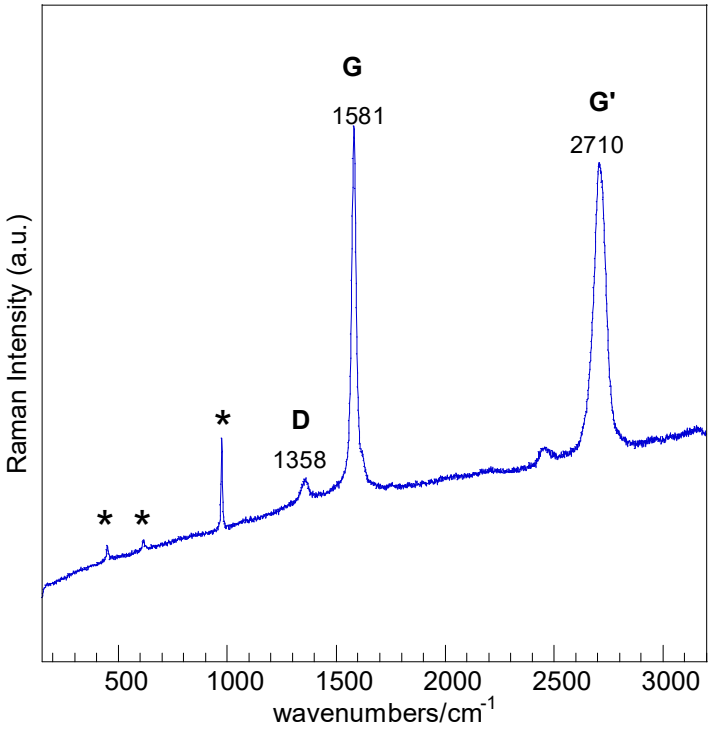

Figure 2. Typical Raman spectrum of carbon nanotubes spots. Bands marked by a star (*) are due to sulfates impurities. D, G, G' are the typical D, G and G' bands, respectively.

3.3. Electrochemical Characterization

The electrochemical behavior of both Au bare and Au-modified electrodes was studied using two electrochemical techniques, cyclic voltammetry (CV) and electrochemical impedance spectroscopy (EIS), able to characterize the reversibility of the electron transfer process and the charge transfer resistance at the electrode-solution interface, respectively. The redox couple $Fe(CN)_6^{3-/4-}$ was used as anionic electrochemical probe for examining the different platforms [58,61].

3.3.1. Cyclic Voltammetry Characterization

The unmodified and modified Au electrodes were electrochemically characterized by using cyclic voltammetry experiments in a solution containing 5 mM $[Fe(CN)^6]^{3-/4-}$ and 0.1 M KCl, at a scan rate of 50 mV s^{-1}. Figure 3 shows the CV profiles of the bare, Au/SWCNTs and h-nPG gold electrodes, respectively. All CVs show a couple of redox peaks with a large increase of the anodic and cathodic peak currents and a decrease of the peak-to-peak separation (ΔE_p), after electrode modifications, due to the increase of the electroactive surface area and reversibility of the systems, in both cases. The highest anodic and cathodic peak currents were observed with h-nPG electrode, together with the lowest ΔE_p value of about 87 mV, close to the theorical ΔE_p value (59 mV), typical of a monoelectronic reversible mediator.

In addition, the effect of the scan rate on the current responses of the h-nPG electrode has been evaluated. Figure 4 shows the CVs corresponding to different scan rates from 5 to 500 mV s^{-1} and the linear relationship between the peak current values and the square root of the scan rate. The corresponding linear equations for the anodic and cathodic peak currents are I_{pa} (A) $= -3.02 \times 10^{-5} + 3.67 \times 10^{-4}\ v^{1/2}$ ($V \cdot s^{-1}$) with the square of correlation coefficient $R^2 = 0.994$, and I_{pc} (A) $= 3.20 \times 10^{-5} + 3.76 \times 10^{-4}\ v^{1/2}$ ($V \cdot s^{-1}$) with $R^2 = 0.992$. These results attest a diffusion-controlled mass transfer process at the solution/h-nPG interface.

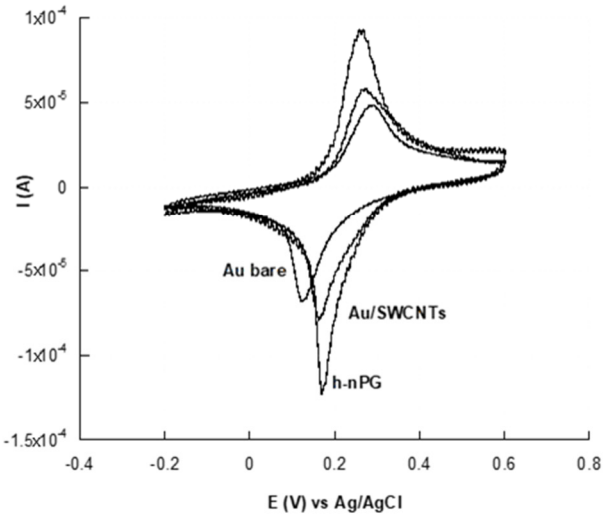

Figure 3. CVs for Au bare (solid line), Au/SWCNTs (dashed line) and h-nPG (dotted line) gold electrodes in 5 mM $[Fe(CN)^6]^{3-/4-}$ and 0.1 M KCl, υ = 100 mV s^{-1}.

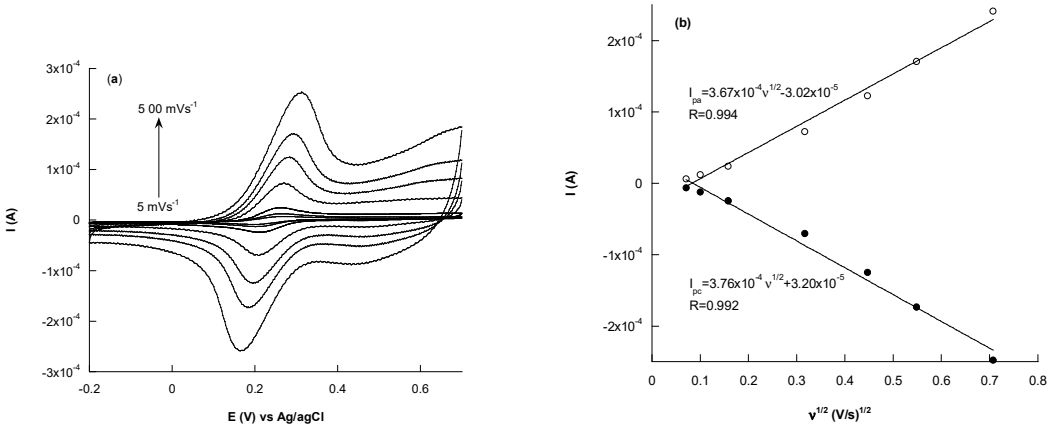

Figure 4. CVs (**a**) of h-nPG electrode at different scan rates (5, 10, 25, 100, 200, 300, 500 mVs^{-1}) and (**b**) the corresponding peak currents vs. the square root of scan rate in 5 mM $[Fe(CN)^6]^{3-/4-}$ and 0.1 M KCl.

All electroanalytical parameters before and after electrode modifications, such as ΔE_p, electroactive areas (A_e), ρ values and the heterogeneous electron transfer rate constants (k_0) of the bare and the modified electrodes are reported in Table 1. In particular, the electroactive area (A_e) of Au/SWCNTs and h-nPG electrodes resulted to be about 14 and 20 times larger than that reported for the bare electrode. This behavior can be ascribed to the nano-structuration obtained with carbon nanotubes and to the 3D-network of the h-nPG, which improves the electron transfer rate between the electrode surface and the bulk solution. Consequently, the roughness factors ρ values reported in Table 1 increased accordingly.

Table 1. Comparison of electroanalytical parameters before and after Au electrode modifications. $A_{g\ Au\ bare}$ = 3.10 mm^2.

Sensor	E_{ox}/mV	E_{red}/mV	ΔE_p/mV	A_e (mm^2)	k_0 (cm s^{-1})	ρ
Au bare	283	126	157	2.86	0.85×10^{-3}	0.92
Au/SWCNTs	270	164	106	39.90	2.95×10^{-3}	13.31
h-nPG	263	176	87	59.20	3.98×10^{-3}	19.10

The A_e values have been evaluated using the Randles-Sevcik equation [60], which for a reversible process is as follows:

$$Ip = 2.686 \times 10^5 \, n^{3/2} \, A_e \, D_0{}^{1/2} \, C_0 \, \upsilon^{1/2} \quad (1)$$

where I_p is the voltammetric peak current (A), n the number of electrons ($n = 1$), A_e the electroactive area (cm^2), D_0 the diffusion coefficient (7.6×10^{-6} cm^2 s^{-1} for ferricyanide), C_0 the concentration (mol cm^{-3}), and υ the scan rate (Vs^{-1}). In particular, the A_e values were calculated by using the slope of the plot I_p vs $\upsilon^{1/2}$ for each electrode. The heterogeneous electron transfer rate constant (k_0) values were calculated using the extended method obtained by merging Klingler-Kochi and Nicholson-Shain methods, for totally irreversible and reversible systems, respectively [62–65], and the roughness factors (ρ) from the ratio of the electroactive (A_e) to the geometric area (A_g) of each electrode.

It is interesting to note that the k_0 value obtained in the case of Au/SWCNTs and h-nPG electrodes resulted to be about four and five times higher than that obtained with Au bare electrode, respectively, showing a relatively faster electron transfer kinetics, thanks to the high conductivity of the gold nanostructures. Compared to the 20-times increase in the electroactive area obtained with h-nPG electrode, the corresponding increase in the k_0 value is quite limited. This can be ascribed to the fact that the $[Fe(CN)^6]^{3-/4-}$ redox probe has a fast kinetics and therefore its concentration at the outerpore rapidly drops to zero without leaving to the redox probe enough time to reach the inner pore surface which is not "utilized".

3.3.2. Electrochemical Impedance Spectroscopy Characterization

EIS measurements were carried out for further characterization of the modified electrodes. Figure 5 shows the Nyquist plots for the Au bare and the modified Au/SWCNTs and h-nPG electrodes in 0.1 M KCl containing 5.0 mM $Fe(CN)_6{}^{3-/4}$. It is known that the Nyquist plot consists of a semi-circular part at high frequencies, which diameter represents the charge transfer resistance R_{ct}, and a linear part at low frequencies, indicative of systems with diffusion-controlled current [64]. The semicircle diameter depends on the dielectric and insulating features at the electrode-electrolyte interface and can reveal its properties. The EIS data were fitted and the corresponding equivalent circuits are reported in Figure 6. A classical Randles circuit was successfully applied to fit Au bare (Figure 6, circuit (b)), while circuit (a) was proposed for better fitting both h-nPG and Au/SWCNTs modified electrodes.

As can be seen in Figure 5, the largest semicircle was obtained with the Au bare electrode, which corresponds to a R_{ct} value of 1540 Ω (Figure 3, panel a). The R_{ct} value progressively decreases with electrode modification, obtaining a R_{ct} value of 92 Ω with Au/SWCNTs (panel b) and of 1×10^{-6} Ω with h-nPG electrode (panel c), indicating a higher electron transfer rate in the redox probe, thanks to the conductivity of the gold nanostructures. This effect is particularly evident with the h-nPG modified electrode in the low-frequency region, probably because of the interconnected nanoporous structure, suitable for facile electron transport.

The results of the electrochemical fitting by the equivalent circuits are reported in Table 2. Moreover, the kinetic parameters i_0 (exchange current) and k_0 (electron transfer rate constant) have been also determined by EIS measurements [64], using the equations $R_{ct} = RT/nF \, i_0$ and $i_0 = nFAk \, ^\circ C$, where C is the concentration of the redox probe (mol cm^{-3}) and A the electrode area (cm^2). These results are in perfect agreement with the kinetic parameters obtained by cyclic voltammetry discussed in the previous paragraph. It is interesting to note that with this method the k_0 value for the h-nPG electrode was not evaluated, being the process diffusion-controlled only (Figure 5, panel c).

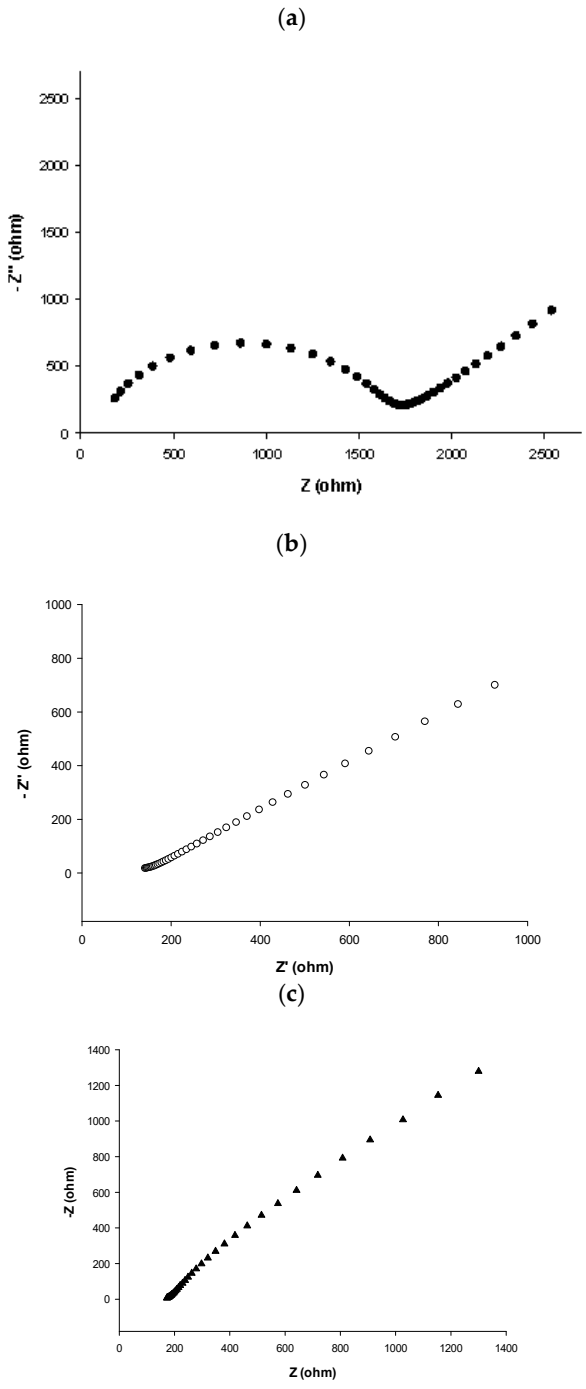

Figure 5. The Nyquist plots of Au bare (**a**), Au/SWCNT (**b**) and h-nPG (**c**) electrodes in 0.1 M KCl containing 5.0 mM $Fe(CN)_6^{3-/4-}$.

(**a**) (**b**)

Figure 6. Equivalent circuits used for fitting the experimental data: circuit (**a**) for h-nPG modified electrode and Au/SWCNTs modified electrode (Randles circuit), and circuit (**b**) for Au bare electrode.

Table 2. EIS results from the electrochemical Nyquist plots fitting.

Sensor SPE	R_s/Ω	R_{ct}/Ω	W/ohm $s^{1/2}$	CPE/ohm s^{N}	N	C_{dl}/F	k_0 (cm s^{-1}) *	i_0 (A) *
Au bare	97	1540	981×10^{-6}	1×10^{-6}	0.9	-	1.21×10^{-3}	16.7×10^{-6}
Au/SWCNTs	76	92	896×10^{-6}	2.74×10^{-4}	0.3	-	1.4×10^{-3}	279×10^{-6}
h-nPG	181	1×10^{-6}	708×10^{-6}	-	-	90×10^{-6}	-	-

* obtained by using a [R(Q[RQ])] modified Randles circuit for diffusionless electrode processes.

3.4. L-Ascorbic Acid Sensor

The electrochemical response of AA in 0.1 M phosphate buffer pH = 7.0 has been investigated by cyclic voltammetry at bare and modified gold electrodes, as reported in Figure 7. All CVs show an irreversible reaction without the cathodic peak in the reverse scan, according to the following reaction mechanism, which involves the release of two electrons and two protons [27]:

$$AA \rightarrow \text{dehydro-AA} + 2H^+ + 2e^- \quad (2)$$

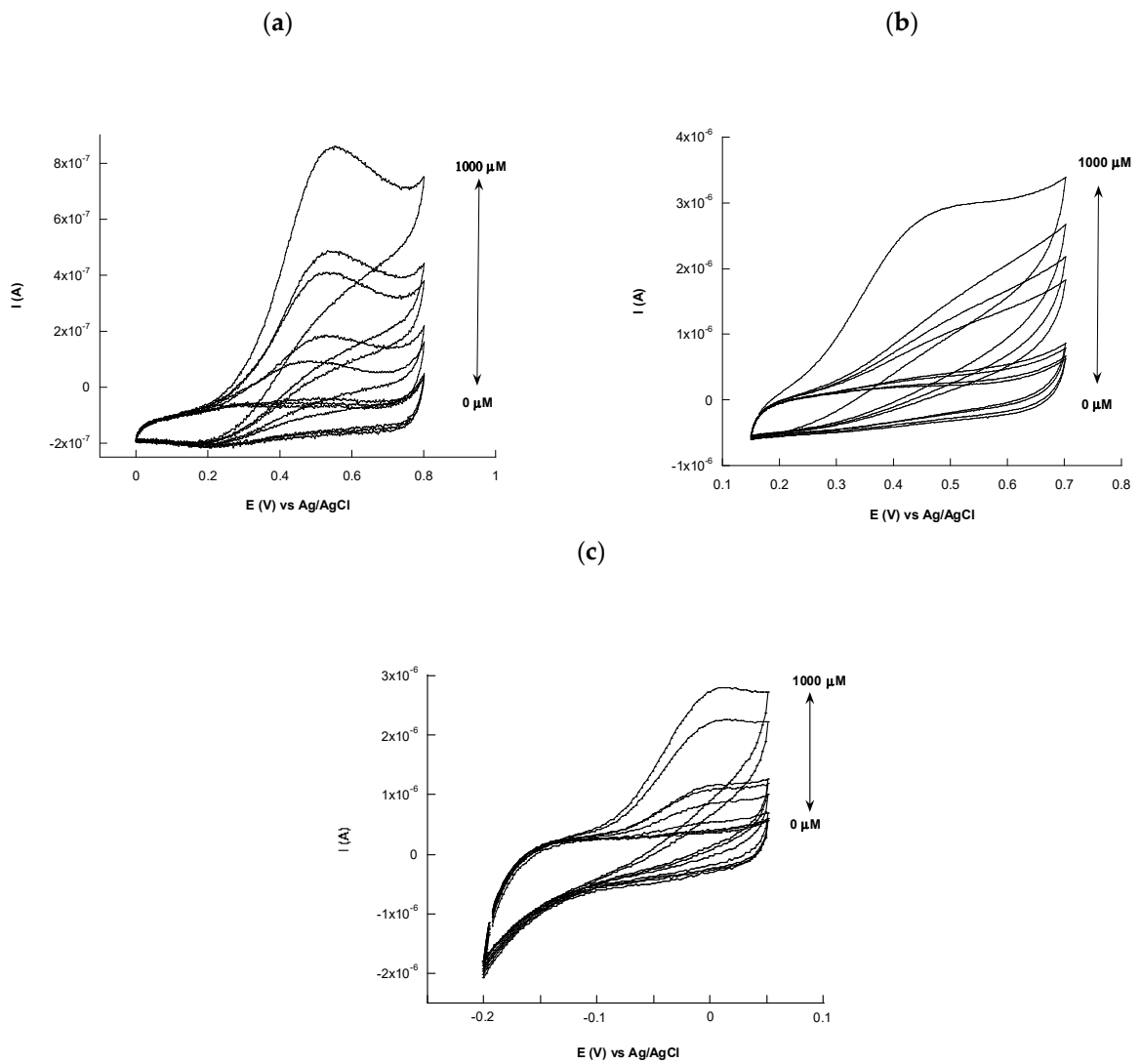

Figure 7. CVs of Au bare (**a**), Au/SWCNTs (**b**) and h-nPG (**c**) electrodes in 0.1 M PBS buffer (pH 7.4), 0.1 M KCl in absence and in presence of different concentrations of AA (0; 10; 25; 150; 200; 400; 800; 1000 M), at υ = 10 mV s^{-1}.

It appears evident that both peak current and peak position of AA oxidation change with the modification of the electrode surface. Anodic peak currents obtained with Au/SWCNTs and h-nPG modified electrodes exhibit higher peak currents and less positive peak potentials than observed at bare electrode. In particular, the peak current potential of AA oxidation at a bare Au electrode occurs at about 0.55 V vs Ag/AgCl (Figure 7, panel a), decreasing to 0.45 V at Au/SWCNTs electrode (panel b) and to 0 V in the case of h-nPG electrode (panel c). The positive potential shifts accompanied by an increase in the peak currents of AA oxidation show that the modified electrodes have a catalytic effect towards AA oxidation, being the catalytic effect of h-nPG electrode stronger than Au/SWCNTs electrode. This result is consistent with the "discriminative amplification" described by Park et al. [47], which occurs at nanoporous electrodes. The AA exhibits a slow kinetics [66,67] and therefore the AA concentration at the outerpore does not fall to zero and the AA oxidation takes place deeper inside the nanopores. Moreover, structural defects and the low index crystalline faces in inner surface of the pores play a dominant role in enhancing the electron transfer rate [50,68,69]. These effects can explain the improved electron transfer kinetics with the marked shift of the anodic peak potential towards more negative values.

As the oxidation reaction of AA is accompanied by a two-proton transfer (reaction 1) [68], which is facilitated at higher pH values, it is possible that an increase in the pH value would increase the peak currents and shift the peak potentials towards more negative values, as already reported by some authors [40,70–72]. Nevertheless, a pH value of 7.4 in 0.1 M phosphate buffer has been chosen in this study, as it is closer to physiological conditions.

Figure 8 shows the linear part of the calibration curves of the modified AA sensors (curves B and C). The calibration curve of the bare Au sensor was reported as comparison (curve A). The linear equations for the three electrodes are listed as follows:

$$\text{Ip } (\mu\text{A}) = 0.001\ C_{AA}\ (\text{M}) - 0.07,\ R^2 = 1$$
$$\text{Ip } (\mu\text{A}) = 0.002\ C_{AA}\ (\text{M}) + 0.22,\ R^2 = 0.99$$
$$\text{Ip } (\mu\text{A}) = 0.003\ C_{AA}\ (\text{M}) + 0.29,\ R^2 = 0.98$$

The three electrodes showed the same linear range between 5 and 400 μM, with a detection limit (S/N = 3) of 3.8, 3.1 and 1.8 μM for the bare, Au/SWCNTs and h-nPG modified electrode, respectively. The linear range is relatively extended, but it covers the normal range of AA concentration in human urine. The sensitivity resulted strongly enhanced with both nanostructured modified electrodes compared to bare electrode, resulting to be 1.7×10^{-2} μA $\mu M^{-1} cm^{-2}$ and 2.5×10^{-2} μA $\mu M^{-1} cm^{-2}$ for Au/SWCNTs and h-nPG, respectively, about 2 times higher values than that determined for the bare gold electrode (1.0×10^{-2} μA $\mu M^{-1} cm^{-2}$).

The h-nPG based sensor showed the highest sensitivity and was therefore chosen for further characterization. The more sensitive differential pulse voltammetry (DPV) technique was also performed with the h-nPG modified electrode. DP voltammograms are reported at different concentration of AA in Figure S1 (Supplementary Materials). The electrode sensitivity resulted to be higher with a linear range linear fitted by equation: I (mA) = 0.01 [AA] (mM) + 11, $R^2 = 0.991$ between 2 and 800 μM.

It is interesting to underline that very few nPG based sensors have been reported in literature for AA detection. El-Said and Qiu [73,74] used an electrochemical deposition and dealloying method, respectively, for the fabrication of nPG sensors for dopamine (DA) detection in the presence of AA. Differential pulse voltammetry experiments showed two well-separated oxidation peaks, allowing the selective determination of DA in the presence of AA with both sensors, but the aim of these works was the detection of DA, being AA studied only as a possible interferent at a fixed concentration.

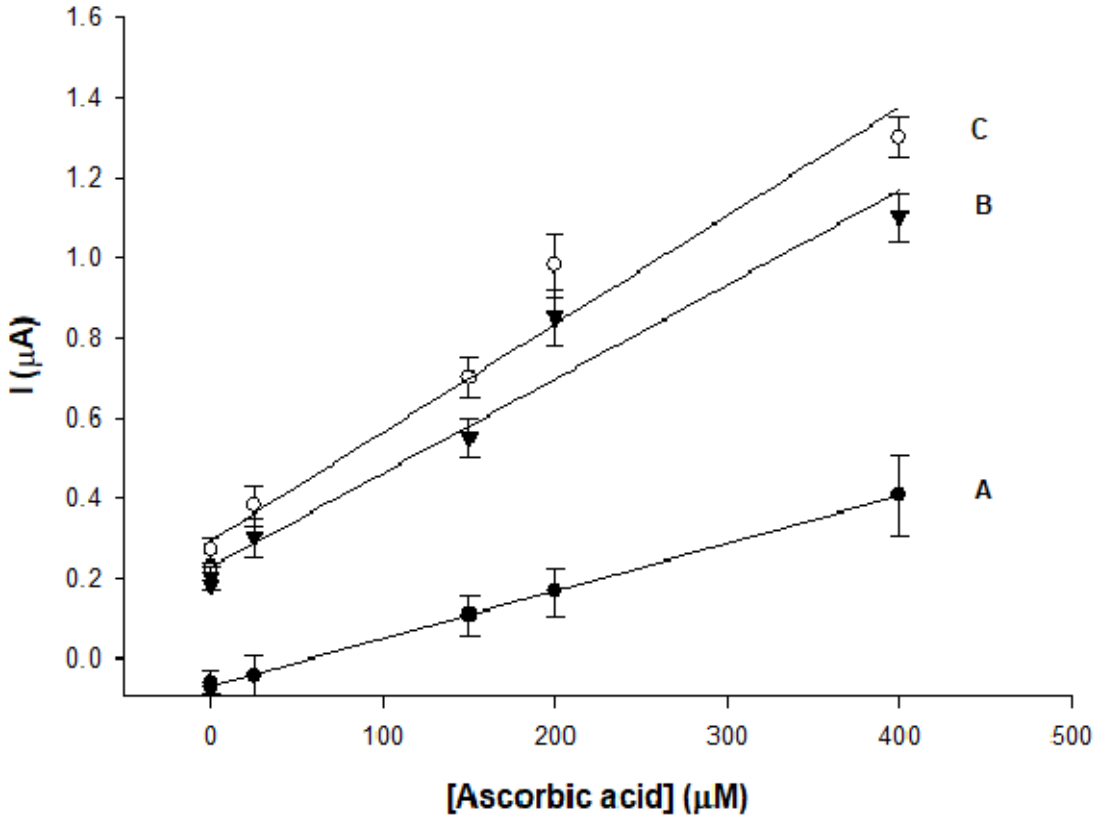

Figure 8. Calibration curves of Au bare (**A**), Au/SWCNTS (**B**) and h-nPG (**C**) modified electrodes in 0.1 M PBS pH = 7.4, KCl = 0.1 M.

Most sensors for AA detection recently reported in literature have been realized through the development of efficient strategies for the modification and/or functionalization of novel electrochemical platforms, based on conductive polymers, metal oxides, metallic nanoparticles and other nanomaterials, such as carbon nanotubes and graphene, or on their combination for a synergistic effect, as reported in Table 3. The proposed h-nPG sensor shows a clear enhancement of the electrochemical performances, in terms of lower detection limit, extended linear range and better stability, compared to other h-nPG based AA sensors reported in literature, as reported in the first three rows of Table 3. Nevertheless, it exhibits a lower sensitivity and a higher LOD value when compared to classical glassy carbon electrodes modified with metal nanocomposite materials [75–81]. On the other hand, these sensors have known drawbacks, such as long and complex synthesis of metal nanoparticles, drop casting of the nanomaterial onto the electrode surface, resulting in different loading causing poor reproducibility and stability, and electrode surface biofouling. Conversely, the h-nPG based electrodes have the advantage to show strong antibiofouling features [32] and to be prepared by a simple, fast and reproducible electrodeposition method.

Table 3. Comparison of the analytical performances of recently developed AA sensors.

Modified Electrode	Linear Range (μM)	LOD (μM)	Sensitivity (μA μM^{-1} cm^{-2})	Stability	Ref.
h-nPG/AuE (dealloying)	320–3400	63.0	-	-	[32]
h-nPG/AuE (electrodeposition)	10–1100	2	-	88% after 5 weeks	[28]
h-nPG/AuE (electrodeposition)	5–400	1.8	2.5×10^{-2}	98% after 1 month	this work
PVP-GR/GCE	4–1000	0.8	-	83.6% after 15 days	[75]
rGO/Fe_3O_4/HP-ß-CD/GCE	10–350	3.3	-	~100% after 1 month	[76]
P(Arg)-GO/AgNPs/GCE	4–2400	0.9	-	-	[77]
Au-PDNs/SPCE	10–240	0.2×10^{-3}	2.2×10^{-2}	~99% after 2 months	[78]
AgNC@PDA-NS/AuE	50–4000	6.4	8.4×10^{-2}	-	[79]
rGO-poly(PR)/AuNPs/GCE	0.4–110	0.054	4.9	87.5% over 1 month	[80]
GO/$TmPO_4$/GCE	0.06–100	0.4	0.239	92.33% after 2 weeks	[81]
poly-TB/GCE	1–630	0.1	0.46	97.9% after 3 weeks	[39]

List of abbreviations: AuE = gold electrode; PVP = polyvinylpyrrolidone; GCE = glassy carbon electrode; rGO = reduced graphene oxide; HP-ß-CD = hydroxypropyl-b-cyclodextrin; P(Arg) = poly(L-arginine); GO = graphene oxide; AgNPs = silver nanoparticles; Au-PDNs = gold decorated-polydopamine nanospheres; SPCE = screen-printed carbon electrode; AgNC = silver nanocube; PDA-NS = polydopamine nanospheres; poly(PR) = Procion Red MX-5B; $TmPO_4$ = thulium phosphate; poly-TB = poly-Trypan Blue.

3.5. Reproducibility and Stability

The reproducibility of the h-nPG sensor was evaluated and expressed as relative standard deviation (RSD) for $n = 8$, where n represents the number of sensors used for the test of 10 μM of AA. The RSD value was found 2.54%, attesting that the highly reproducibility of the method.

The stability of the proposed sensor was also studied by measuring the anodic peak current variations of each sensor when stored in pH 7.4 PBS for 1 month at 4 °C. The anodic peak current retained about 98% of its initial value.

3.6. Interference Studies

The selectivity of the h-nPG sensor was tested by evaluating the effects of several interfering compounds present in biological fluids on the determination of 100 M AA. Initially, the interference of dopamine (DA) and uric acid (UA) were investigated, as they frequently coexist in biological systems. They are easily oxidized at most conventional electrodes at closed potentials, showing overlapping voltammetric signals. The anodic peaks of AA, DA and UA overlapped at about 0.5 V vs. Ag/AgCl at bare gold electrodes (curves not shown), while at h-nPG electrode the anodic peaks appear well resolved with peak potentials at 0, 0.20 and 0.32 V vs. Ag/AgCl, respectively, as reported in Figure 9, thus not affecting the AA detection. The anodic shift of the peak potentials of AA, DA and UA, which allows their selective determination, can be explained by taking into account that, AA, DA and UA show slow electron transfer reactions [32,47,66]. The concentration of their oxidized forms at the outerpore does not fall to zero, meaning that the reduction of the oxidized species takes place deeper inside the nanopores. This "nanoconfinement effect" results in an improvement of the electron transfer kinetics with a concomitant anodic shift of the peak potentials.

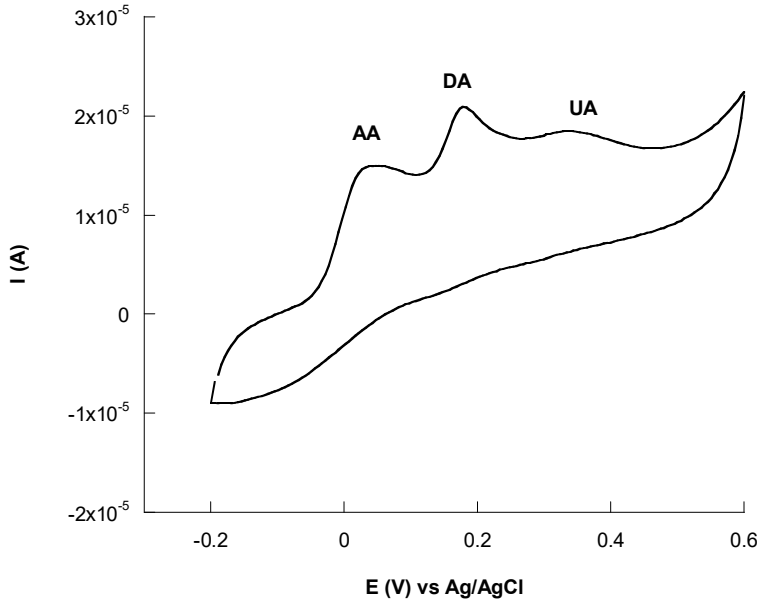

Figure 9. Cyclic voltammograms of AA 4 mM + DA 3 mM and UA 6 mM at h-nPG electrode in 0.1 M PBS pH = 7.4, KCl = 0.1 M, at υ = 10 mV s^{-1}.

Successively, other possible interfering species such as glucose, L-cysteine, L-lysine, urea, and citric acid were checked by adding equal quantities of the interferent and AA. The results are shown in Table 4. No significant influence was observed for all interferences with a relative error lower than 5%.

Table 4. Influence of interfering compounds on AA response of the h-nPG sensor. Interference amount added = 500 M.

Interfering Compound	[AA] (M)	Recovery (%)
Glucose	480	95
L-cysteine	490	98
L-lysine	495	99
Urea	475	95
citric acid	485	97

3.7. Real Samples Analysis

The feasibility of the proposed h-nPG sensor for clinical applications was tested by detecting the AA concentration in human urine samples by using the low cost and easy-to-use SPEs. The only sample pretreatment required was a proper dilution (1:10^3) of the urine samples using 0.1 M PBS pH = 7 in order to fit the linear range of the sensor. Different concentrations of AA were added to three human urine samples supplied from laboratory co-workers. All measurements were performed on a triplicate basis and the results were compared with those obtained with a standard spectrophotometric method, by following the absorbance at 570 nm. As shown in Table 5, the results obtained with the two methods resulted in a very good agreement and allowed to ascertain the practical utility of the proposed sensor for the detection of AA in human urine samples.

Table 5. Detection of AA in real human urine samples with h-nPG modified SPEs.

Urine Sample	Added (M)	Detected (M)	Spectrophotometric Method (M)	Recovery (%)
1	10.0	10.56	10.34	105.6 ± 0.72
2	20.0	21.16	20.86	105.8 ± 1.22
3	50.0	49.20	50.88	98.40 ± 0.29

4. Conclusions

Two novel electrochemical sensors based on gold electrodes modified with Au/SWCNTs and h-nPG have been realized and utilized for the detection of AA. Both CV and EIS experiments confirmed the high electrochemical performances of the modified electrodes, compared to the bare gold electrode. AA was determined in the linear range 5–400 μM with detection limits of 3.1 and 1.8 μM, with Au/SWCNTs and h-nPG modified sensor, respectively. The higher sensitivity showed by the h-nPG electrode over the bulk gold and Au/SWCNTs electrodes can be attributed to the unique, highly curved morphology that permeates the material, exhibiting a high density of steps and holes, which can facilitate the electron transfer of AA.

Another strength of the proposed h-nPG electrode is its easy preparation method, by a self-templated electrodeposition technique, compared to the dealloying methods reported in literature for the fabrication of h-nPG electrodes for AA detection [32,74,80,81] which means the harsh conditions needed for chemical dealloying can be avoided.

Moreover, the h-nPG sensor was successfully tested with disposable SPEs, properly modified, for accurate detection of AA in human urine samples, with satisfactory results, showing high recovery values. For these reasons, the proposed sensor may have promising potential applications for non-invasive, reliable, fast, cheap and accurate monitoring of AA at the POC.

Supplementary Materials: The following are available online at https://www.mdpi.com/article/10.3390/chemosensors9080229/s1, Figure S1: DP voltammograms recorded in 0.1 M PBS pH = 7.4, KCl = 0.1 M at different concentrations of AA (10, 150, 250, 400, 800 mM) using h-nPG electrode. Inset: calibration curve of AA.

Author Contributions: Investigation, C.T.; methodology, C.T. and F.T.; validation, M.A.V.; supervision, R.A. and C.M.; writing original draft, R.A. All authors have read and agreed to the published version of the manuscript.

Funding: This research received no external funding.

Conflicts of Interest: The authors declare no conflict of interest.

References

1. Iqbal, K.; Khan, A.; Khattak, M. Biological significance of ascorbic acid (vitamin C) in human health—A review. *Pak. J. Nutr.* **2004**, *3*, 5–13.
2. Davies, M.B.; Partridge, D.A.; Austin, J.A. *Vitamin C: Its Chemistry and Biochemistry*; The Royal Society of Chemistry: Cambridge, UK, 1991.
3. Arrigoni, O.; De Tullio, M.C. Ascorbic acid: Much more than just an antioxidant. *Biochim. Biophys. Acta Gen. Subj.* **2002**, *1569*, 1–9. [CrossRef]
4. Padayatty, S.J.; Katz, A.; Wang, Y.H.; Eck, P.; Kwon, O.; Lee, J.H.; Chen, S.L.; Corpe, C.; Dutta, A.; Dutta, S.K.; et al. Vitamin C as an antioxidant: Evaluation of its role in disease prevention. *J. Am. Coll. Nutr.* **2003**, *22*, 18–35. [CrossRef] [PubMed]
5. Carr, A.C.; Maggini, S. Vitamin C and immune function. *Nutrients* **2017**, *9*, 1211. [CrossRef]
6. Hemilä, H. Vitamin C supplementation and the common cold—Was Linus Pauling right or wrong? *Int. J. Vitam. Nutr. Res.* **1997**, *67*, 329–335. [PubMed]
7. Hemilä, H.; Chalker, E. Vitamin C for preventing and treating the common cold. *Cochrane Database Syst. Rev.* **2013**, *1*. [CrossRef]
8. Massey, L.K.; Liebman, M.; Kynast-Gales, S.A. Ascorbate increases human oxaluria and kidney stone risk. *J. Nutr.* **2005**, *135*, 1673–1677. [CrossRef]
9. Pincemail, J.; Vanbelle, S.; Degrune, F.; Cheramy-Bien, J.P.; Charlier, C.; Chapelle, J.P.; Giet, D.; Collette, G.; Albert, A.; Defraigne, J.O. Lifestyle behaviours and plasma vitamin C and β-carotene levels from the ELAN population (Liège, Belgium). *J. Nutr. Metab.* **2011**, *2011*, 494370. [CrossRef]
10. Biancatelli, R.M.L.C.; Berrill, M.; Marik, P.E. The antiviral properties of vitamin C. *Expert Rev. Anti-Infect. Ther.* **2020**, *18*, 99–101. [CrossRef]
11. Cerullo, G.; Negro, M.; Parimbelli, M.; Pecoraro, M.; Perna, S.; Liguori, G.; Rondanelli, M.; Cena, H.; D'Antona, G. The long history of vitamin C: From prevention of the common cold to potential aid in the treatment of COVID-19. *Front. Immunol.* **2020**, *11*, 574029. [CrossRef]
12. Carr, A.C.; Roew, S. The emerging role of vitamin C in the prevention and treatment of COVID-19. *Nutrients* **2020**, *12*, 3286. [CrossRef] [PubMed]

13. Zhang, J.; Rao, X.; Li, Y.; Zhu, Y.; Liu, F.; Guo, G.; Luo, G.; Meng, Z.; Backer, D.D.; Xiang, H.; et al. Pilot trial of high-dose vitamin C in critically ill COVID-19 patients. *Ann. Int. Care* **2021**, *11*, 5. [CrossRef]
14. Law, W.S.; Kubáň, P.; Zhao, J.H.; Li, S.F.Y.; Hauser, P.C. Determination of vitamin C and preservatives in beverages by conventional capillary electrophoresis and microchip electrophoresis with capacitively coupled contactless conductivity detection. *Electrophoresis* **2005**, *26*, 4648–4658. [CrossRef]
15. Wu, T.; Guan, Y.; Ye, J. Determination of flavonoids and ascorbic acid in grapefruit peel and juice by capillary electrophoresis with electrochemical detection. *Food Chem.* **2007**, *100*, 1573–1579. [CrossRef]
16. Jain, A.; Chaurasia, A.; Verma, K.K. Determination of ascorbic acid in soft drinks, preserved fruit juices and pharmaceuticals by flow injection spectrophotometry: Matrix absorbance correction by treatment with sodium hydroxide. *Talanta* **1995**, *42*, 779–787. [CrossRef]
17. Tabata, M.; Morita, H. Spectrophotometric determination of a nanomolar amount of ascorbic acid using its catalytic effect on copper (II) porphyrin formation. *Talanta* **1997**, *44*, 151–157. [CrossRef]
18. Alwarthan, A.A. Determination of ascorbic acid by flow injection with chemiluminescence detection. *Analyst* **1993**, *118*, 639–642. [CrossRef]
19. Agater, I.B.; Jewsbury, R.A. Direct chemiluminescence determination of ascorbic acid using flow injection analysis. *Anal. Chim. Acta* **1997**, *356*, 289–294. [CrossRef]
20. Chen, H.; Li, R.; Lin, L.; Guo, G.; Lin, J.-M. Determination of l-ascorbic acid in human serum by chemiluminescence based on hydrogen peroxide–sodium hydrogen carbonate–CdSe/CdS quantum dots system. *Talanta* **2010**, *81*, 1688–1696. [CrossRef]
21. Verdini, R.A.; Lagier, C.M. Voltammetric iodometric titration of ascorbic acid with dead-stop end-point detection in fresh vegetables and fruit samples. *J. Agric. Food Chem.* **2000**, *48*, 2812–2817. [CrossRef]
22. Suntornsuk, L.; Gritsanapun, W.; Nilkamhank, S.; Paochom, A. Quantitation of vitamin C content in herbal juice using direct titration. *J. Pharm. Biomed. Anal.* **2002**, *28*, 849–855. [CrossRef]
23. Pachla, L.A.; Kissinger, P.T. Determination of ascorbic acid in foodstuffs, pharmaceuticals, and body fluids by liquid chromatography with electrochemical detection. *Anal. Chem.* **1976**, *48*, 364–367. [CrossRef] [PubMed]
24. Speek, A.; Schrijver, J.; Schreurs, W. Fluorometric determination of total vitamin C in whole blood by high-performance liquid chromatography with pre-column derivatization. *J. Chromatogr. B Biomed. Sci. Appl.* **1984**, *305*, 53–60. [CrossRef]
25. Iwata, T.; Yamaguchi, M.; Hara, S.; Nakamura, M.; Ohkura, Y. Determination of total ascorbic acid in human serum by high-performance liquid chromatography with fluorescence detection. *J. Chromatogr. B Biomed. Sci. Appl.* **1985**, *344*, 351–355. [CrossRef]
26. Perez-Ruiz, T.; Martinez-Lozano, C.; Tomas, V.; Fenol, J. Fluorimetric determination of total ascorbic acid by a stopped-flow mixing technique. *Analyst* **2001**, *126*, 1436–1439. [CrossRef] [PubMed]
27. Pisoschi, A.M.; Pop, A.; Serban, A.I.; Fafaneata, C. Electrochemical methods for ascorbic acid determination. *Electrochim. Acta* **2014**, *121*, 443–460. [CrossRef]
28. Kumar, S.A.; Lo, P.H.; Chen, S.M. Electrochemical selective determination of ascorbic acid at redox active polymer modified electrode derived from direct blue. *Biosens. Bioelectron.* **2008**, *24*, 518–523. [CrossRef] [PubMed]
29. Dhara, K.; Debièrosad, R.M. Review on nanomaterials-enabled electrochemical sensors for ascorbic acid detection. *Anal. Biochem.* **2019**, *586*, 113415. [CrossRef] [PubMed]
30. Tomita, I.N.; Manzoli, A.; Fertonani, F.L.; Yamanaka, H. Amperometric biosensor for ascorbic acid. *Eclét. Quím.* **2005**, *30*, 37–43. [CrossRef]
31. Akyilmaz, E.; Dinçkaya, E. A new enzyme electrode based on ascorbate oxidase immobilized in gelatin for specific determination of L-ascorbic acid. *Talanta* **1999**, *50*, 87–93. [CrossRef]
32. Silva, T.A.; Khan, M.R.K.; Fatibello-Filho, O.; Cillinson, M.M. Simultaneous electrochemical sensing of ascorbic acid and uric acid under biofouling conditions using nanoporous gold electrodes. *J. Electroanal. Chem.* **2019**, *846*, 113160. [CrossRef]
33. Barfidokht, A.; Gooding, J.J. Approaches toward allowing electroanalytical devices to be used in biological fluids. *Electroanalysis* **2014**, *26*, 1182–1196. [CrossRef]
34. Wisniewski, N.; Moussy, F.; Reichter, M.W. Characterization of implantable biosensor membrane biofouling. *Fresenius J. Anal. Chem.* **2000**, *366*, 611–621. [CrossRef]
35. Sha, Y.F.; Qian, L.; Ma, Y.; Bai, H.X.; Yang, X.R. Multilayer films of carbon nanotubes and redox polymer on screen-printed carbon electrodes for electrocatalysis of ascorbic acid. *Talanta* **2006**, *70*, 556–560. [CrossRef]
36. Thangamuthu, R.; Kumar, S.M.; Pillai, K.C. Direct amperometric determination of l-ascorbic acid (vitamin C) at octacyanomolybdate-doped-poly(4-vinylpyridine) modified electrode in fruit juice and pharmaceuticals. *Sens. Actuators B Chem.* **2007**, *120*, 745–753. [CrossRef]
37. Xi, L.; Ren, D.; Luo, J.; Zhu, Y. Electrochemical analysis of ascorbic acid using copper nanoparticles/polyaniline modified glassy carbon electrode. *J. Electroanal. Chem.* **2010**, *650*, 127–134. [CrossRef]
38. Liu, S.; Jiang, X.; Yang, M. Electrochemical sensing of L-ascorbic acid by using a glassy carbon electrode modified with a molybdophosphate film. *Microchim. Acta* **2019**, *186*, 445. [CrossRef]
39. Taei, M.; Jamshidi, M.S. A voltammetric sensor for simultaneous determination of ascorbic acid, noradrenaline, acetaminophen and tryptophan. *Microchem. J.* **2017**, *130*, 108–115. [CrossRef]

40. Pisoschi, A.M.; Danet, A.F.; Kalinowski, S. Ascorbic acid determination in commercial fruit juice samples by cyclic voltammetry. *J. Anal. Methods Chem.* **2008**, *2008*, 1–8. [CrossRef] [PubMed]
41. Hu, G.; Ma, Y.; Guo, Y.; Shao, S. Electrocatalytic oxidation and simultaneous determination of uric acid and ascorbic acid on the gold nanoparticles-modified glassy carbon electrode. *Electrochim. Acta* **2008**, *53*, 6610–6615. [CrossRef]
42. Tig, G.A. Development of electrochemical sensor for detection of ascorbic acid, dopamine, uric acid and L-tryptophan based on Ag nanoparticles and poly(L-argininne)-graphene oxide composite. *J. Electroanal. Chem.* **2017**, *807*, 19–28. [CrossRef]
43. Argoubi, W.; Rabti, A.; Aoun, S.B.; Raouafi, N. Sensitive detection of ascorbic acid using screen-printed electrodes modified by electroactive melanin b-like nanoparticles. *RSC Adv.* **2019**, *9*, 37384–37390. [CrossRef]
44. Arroquia, A.; Acosta, I.; Armada, M.P.G. Self-assembled gold decorated polydopamine nanosphere as electrochemical sensor for simultaneous determination of ascorbic acid, dopamine, uric acid and tryptophan. *Mater. Sci. Eng. C* **2020**, *109*, 110602. [CrossRef] [PubMed]
45. Farghaly, A.A.; Lam, M.; Freeman, C.Y.; Uppalapati, B.; Collinson, M.M. Potentiometric measurements in biofouling solutions: Comparison of nanoporous gold to planar gold. *J. Electroanal. Soc.* **2016**, *163*, H3083–H3087. [CrossRef]
46. Jena, B.K.; Ray, C.R. Morphology dependent electrocatalytic activity of Au nanoparticles. *Electrochem. Commun.* **2008**, *10*, 951–954. [CrossRef]
47. Park, S.; Kim, H.C.; Chung, T.D. Electrochemical analysis based on nanoporous structures. *Analyst* **2012**, *137*, 3891–3903. [CrossRef] [PubMed]
48. Daggumati, P.; Matharu, Z.; Wang, L.; Seker, E. Biofouling resilient nanoporous gold electrodes for DNA sensing. *Anal. Chem.* **2015**, *87*, 8618–8622. [CrossRef]
49. Collinson, M. Nanoporous gold electrodes and their applications in Analytical Chemistry. *Int. Sch. Res. Not. Anal. Chem.* **2013**, *2013*. [CrossRef]
50. Wittstock, A.; Biener, J.; Baumer, M. *Introduction to Nanoporous Gold*; Royal Society of Chemistry: London, UK, 2012.
51. Bollella, P.; Hibino, Y.; Kano, K.; Gorton, L.; Antiochia, R. Highly sensitive membraneless fructose biosensor based on fructose dehydrogenase immobilized onto aryl thiol modified highly porous gold electrode: Characterization and application in food samples. *Anal. Chem.* **2018**, *90*, 12131–12136. [CrossRef]
52. Junior, G.J.S.; Selva, J.S.G.; Sukeri, A.; Goncalves, J.M.; Regiart, M.; Bertotti, M. Fabrication of dendritic nanoporous gold via a two-step amperometric approach: Application for electrochemical detection of methyl parathion in river water samples. *Talanta* **2021**, *226*, 122130. [CrossRef]
53. Plowman, B.J.; Jones, L.A.; Bhargava, S.K. Building with bubbles: The formation of high surface area honeycomb-like films via hydrogen bubble templated electrodeposition. *Chem. Commun.* **2015**, *51*, 4331–4346. [CrossRef] [PubMed]
54. Kumar, A.; Furtado, V.L.; Goncalves, J.M.; Bannitz-Fernandes, R.; Netto, L.E.-S.; Araki, K.; Bertotti, M. Amperometric microsensor based on nanoporous gold for ascorbic acid detection in highly acidic biological extracts. *Anal. Chim. Acta* **2020**, *2095*, 61–70. [CrossRef] [PubMed]
55. Sanzó, G.; Taurino, L.; Antiochia, R.; Gorton, L.; Favero, G.; Mazzei, F.; De Micheli, G.; Carrara, S. Bubble electrodeposition of gold porous nanocorals for the enzymatic and non-enzymatic detection of glucose. *Bioelectrochemistry* **2016**, *112*, 125–131. [CrossRef]
56. Bollella, P.; Sharma, S.; Cass, A.E.G.; Antiochia, R. Microneedle-based biosensor for minimally-invasive lactate detection. *Biosens. Bioelectron.* **2019**, *123*, 152–159. [CrossRef] [PubMed]
57. Dai, X.; Compton, R.G. Direct electrodeposition of gold nanoparticles onto indium tin oxide film coated glass: Application to the detection of arsenic (III). *Anal. Sci.* **2006**, *22*, 567–570. [CrossRef] [PubMed]
58. Bollella, P.; Sharma, S.; Cass, A.E.G.; Tasca, F.; Antiochia, R. Minimally invasive glucose monitoring using a highly porous gold microneedles-based biosensor: Characterization and application in artificial interstitial fluid. *Catalysts* **2019**, *9*, 580. [CrossRef]
59. Jorio, A.; Saito, R. Raman spectroscopy for carbon nanotube applications. *J. Appl. Phys.* **2021**, *129*, 021102–021127. [CrossRef]
60. Ben, K.; Kauffmann, H.; Aroui, H.; Fontana, M. Raman study of cation effect on sulfate vibration modes in solid state and in aqueous solutions. *J. Raman Spectrosc.* **2013**, *44*, 1603–1608.
61. Pina, S.; Candia-Onfray, C.; Hassan, N.; Jara-Ulloa, P.; Contreras, D.; Salazar, R. Glassy carbon electrode modified with C/Au nanostructured materials for simultaneous determination of hydroquinone and cathecol in water matrices. *Chemosensors* **2021**, *9*, 88. [CrossRef]
62. Oldham, K.B. Analytical expressions for the reversible Randles-Sevcik function. *J. Electroanal. Chem. Interfacial Electrochem.* **1979**, *105*, 373–375. [CrossRef]
63. Lavagnini, I.; Antiochia, R.; Magno, F. An extended method for the practical evaluation of the standard rate constant from cyclic voltammetric data. *Electroanalysis* **2004**, *16*, 505–506. [CrossRef]
64. Lavagnini, I.; Antiochia, R.; Magno, F. A calibration-base method for the evaluation of the detection limit of an electrochemical biosensor. *Electroanalysis* **2007**, *19*, 1227–1230. [CrossRef]
65. Bard, A.J.; Faulkener, L.R. *Electrochemical Methods, Fundamentals and Applications*, 2nd ed.; John Wiley & Sons, Inc.: New York, NY, USA, 2001; p. 381.
66. Randviir, E.P. A cross examination of electron transfer rate constants for carbon screen-printed electrodes using Electrochemical Impedance Spectroscopy and cyclic voltammetry. *Electrochim. Acta* **2018**, *186*, 179–186. [CrossRef]
67. Jiang, D.; Li, X.; Liu, L.; Yagnik, G.B.; Zhou, F. reaction rates and mechanism of the ascorbic acid oxidation by molecular oxygen facilitated by Cu(II)-containing amyloid-β complexes and aggregates. *J. Phys. Chem. B* **2010**, *114*, 48–96. [CrossRef]

68. Kumar, A.; Gonçalves, J.M.; Selva, J.S.G.; Araki, K.; Bertotti, M. Correlating selective electrocatalysis of dopamine and ascorbic acid electrooxidation at nanoporous gold surfaces with structural-defects. *J. Electrochem. Soc.* **2019**, *166*, H704. [CrossRef]
69. De, S.K.; Mondal, S.; Sen, P.; Pal, U.; Pathak, B.; Rawat, K.S.; Bardhan, M.; Bhattacharya, M.; Satpati, B.; De, A.; et al. Crystal-defect-induced facet-dependent electrocatalytic activity of 3D gold nanoflowers for the selective nanomolar detection of ascorbic acid. *Nanoscale* **2018**, *10*, 13792. [CrossRef]
70. Alden, J.A.; Compton, R.G. Automated simulation of electrode processes: Quantitative mechanistic analysis via working surface interpolation. *J. Phys. Chem. B* **1997**, *101*, 9741–9750. [CrossRef]
71. Zhang, G.; He, P.; Feng, W.; Ding, S.; Chen, J.; Li, L.; He, H.; Zhang, S.; Dong, F. Carbon nanohors/poly(glycine) modified glassy carbon electrode: Preparation, characterization and simultaneous electrochemical determination of uric acid, dopamine and ascorbic acid. *J. Electroanal. Chem.* **2016**, *760*, 24–31. [CrossRef]
72. Bagheri, H.; Pajooheshpour, N.; Khoshsafar, H. A novel electrochemical platform for sensitive and simultaneous determination of dopamine, uric acid and ascorbic acid based on Fe_3O_4 SnO_2 Gr ternary nanocomposite. *Microchem. J.* **2017**, *131*, 120–129. [CrossRef]
73. El-Said, W.A.; Lee, J.H.; Oh, B.K.; Choi, J.W. 3-D nanoporous gold thin film for the simultaneous electrochemical determination of dopamine and ascorbic acid. *Electrochem. Commun.* **2010**, *12*, 1756–1759. [CrossRef]
74. Qiu, H.-J.; Zhou, G.-P.; Ji, G.-L.; Zhang, Y.; Huang, X.-R.; Ding, Y. A novel nanoporous gold modified electrode for the selective determination of dopamine in the presence of ascorbic acid. *Colloids Surf. B Biointerfaces* **2009**, *69*, 105–108. [CrossRef] [PubMed]
75. Wu, Y.; Deng, P.; Tian, Y.; Feng, J.; Xiao, J.; Li, J.; Liu, J.; Li, G.; He, Q. Simultaneous and sensitive determination of ascorbic acid, dopamine and uric acid via an electrochemical sensor based on PVP-graphene composite. *J. Nanobiotechnol.* **2020**, *18*, 112. [CrossRef] [PubMed]
76. Liang, W.; Rong, Y.; Fan, L.; Zhang, C.; Dong, W.; Li, J.; Niu, J.; Yang, C.; Shuang, S.; Dong, C.; et al. Simultaneous electrochemical sensing of serotonin, dopamine and ascorbic acid by using a nanocomposite prepared from reduced graphene oxide, Fe_3O_4 and hydroxypropyl-ß -cyclodextrin. *Microchim. Acta* **2019**, *186*, 751. [CrossRef] [PubMed]
77. Zhang, W.; Chai, Y.; Yuan, R.; Chen, S.; Han, J.; Yuan, D. Facile synthesis of graphene hybrid tube-like structure for simultaneous detection of ascorbic acid, dopamine, uric acid and tryptophan. *Anal. Chim. Acta* **2012**, *756*, 7–12. [CrossRef]
78. Jalalvand, A.R. Four-dimensional voltammetry: An efficient strategy for simultaneous determination of ascorbic acid and uric acid in the presence of dopamine as uncalibrated interfere. *Sens. Biosens. Res.* **2020**, *28*, 100330. [CrossRef]
79. Li, Y.; Jiang, Y.; Song, Y.; Li, Y.; Li, S. Simultaneous determination of dopamine and uric acid in the presence of ascorbic acid using a gold electrode modified with carboxilated graphene and silver nanocube functionalized polydopamine nanospheres. *Microchim. Acta* **2018**, *185*, 382. [CrossRef]
80. Edris, N.M.M.A.; Abdullah, J.; Kamaruzaman, S.; Sulaiman, Y. Ultrasensitive reduced graphene oxide-poly(procion)/gold nanoparticles modified glassy carbon electrode for selective and simultaneous determination of ascorbic acid, dopamine, and uric acid. *J. Electrochem. Soc.* **2019**, *166*, B664. [CrossRef]
81. Huang, H.; Yue, Y.; Chen, Z.; Chen, Y.; Wu, S.; Liao, J.; Liu, S.; Wen, H. Electrochemical sensor based on a nanocomposite prepared from $TmPO_4$ and graphene oxide for simultaneous voltammetric detection of ascorbic acid, dopamine and uric acid. *Microchim. Acta* **2019**, *186*, 189. [CrossRef]